ELSEVIER

A dispersion force approach to modelling the effect of lift forces on fibre dispersion

O. Melander [a],*, A. Rasmuson [b]

[a] *Applied Mechanics, Metso Paper Sundsvall AB, S-851 94 Sundsvall, Sweden*
[b] *Department of Chemical and Biological Engineering, Chalmers University of Technology, S-412 96 Gothenburg, Sweden*

Abstract

Wood fibres suspended in air were studied whilst flowing through a throttle. Measurements of volume fraction and velocity were compared with results from a two-fluid model simulation. Results from earlier work have shown that the lift forces acting on the individual fibres are of importance for the dispersion of volume fraction. Since the orientation of the individual fibres cannot be determined, a dispersion force was utilised to model the dispersing effect of the lift forces. The addition of a lift dispersion model significantly improved the agreement between measurement and model data.
© 2006 Elsevier Ltd. All rights reserved.

1. Introduction

The transport of wood pulp fibres suspended in gas is of great importance in the Medium Density Fibreboard (MDF), tissue and mechanical pulping industries. This includes processes such as the dry forming of fibre webs, steam separation and pneumatic drying.

Despite the importance, previous work on gas–fibre flows is scarce. Experimental studies on fibre–gas flow have been performed by Ek et al. (1978), Garner and Kerekes (1980), Ljus et al. (2002) and Melander et al. (2006). Ek et al. presented an early attempt to measure fibre velocity and concentration simultaneously using laser doppler anemometry (LDA). Garner and Kerekes and Melander et al. determined flow maps by visual observations. In Ljus et al., a hot film technique to determine the velocity and turbulence characteristics of the gas in a fibre–gas suspension is used. Melander and Rasmuson (2004) presented a method of measuring fibre velocity and volumetric concentration simultaneously, using particle image velocimetry (PIV) combined with an image processing procedure, to determine concentration.

Numerical studies of fibre–gas flow are reported by Ljus and Almstedt (1999) and Ljus (2000). In the first paper, a time-dependent Eulerian two-fluid model is used to calculate fibre transport in a mat-forming device.

---

* Corresponding author. Tel.: +46 60 165837; fax: +46 60 165500.
  E-mail address: olof.melander@metso.com (O. Melander).

Two- and three-dimensional calculations are carried out with and without a turbulence model for the gas phase for different working conditions, fibre concentrations and outlet conditions. The behaviour of the fibres is strongly simplified by assuming that they are rigid, single cylinders without angular rotation. Drag coefficients are taken from the work by Ju and Shambaugh (1994). The calculated results of the flow field are compared with measurements of pressure and velocity. It was found that the particle velocity is not affected as much as the gas velocity by the large pressure variations induced in the system because the relaxation time of the particles is longer than the time scale of the pressure variations. This will result in a slip velocity of the phases. In the work by Ljus (2000), numerical calculations of particle transport in a two-dimensional horizontal channel are performed. The influence of the particles on the turbulence is accounted for, and the calculated results are compared with experimental data. It is found that, for fibres, the gas phase turbulence is damped over the entire cross-section; this is in agreement with experimental results reported by Ljus et al. (2002). Melander and Rasmuson (2005) used a two-fluid model to describe the flow of wood fibres and air. The numerical simulations were compared with the experimental data from Melander and Rasmuson (2004). The comparison showed large discrepancies between model and measurements, which were attributed mainly to the inaccurate description of the dispersing effect of lift forces acting on the fibres. Some ideas regarding the dispersion mechanisms were also presented.

In the more extensively studied field of fibres in water, the fibres are generally considered inertialess (e.g. Jeffery, 1922; Mason, 1950; Cox, 1970; Olson and Kerekes, 1998; Olson, 2001). For fibre–air suspensions, the Stokes number, which is a measure of the particle relaxation time, is several orders of magnitude larger than for fibre–water suspensions. Consequently, the fibre acceleration and rotation due to hydrodynamic interaction with the carrier fluid is much slower in fibre–air suspensions than in fibre–water suspensions.

In the present work, an attempt to model the dispersing effect of lift forces is made. The results are compared with experimental data from Melander and Rasmuson (2004) and numerical results from Melander and Rasmuson (2005). The simulations were performed using the commercial CFD software CFX 5.7.1.

2. Experimental

2.1. Experimental set-up

The measurements were performed in a closed-loop, square channel system (Melander and Rasmuson, 2004), where the fibres were circulated using a centrifugal fan. The dimensions of the channel were 200×200 mm and the total system volume was 1 m^3. A throttle, with opening dimensions of 140×200 mm, was inserted into the system. Two of the channel walls in the region of the throttle were transparent to allow for PIV measurements (Fig. 1). Prior to the throttle was a straight, vertical channel section of approximately 9 m in length.
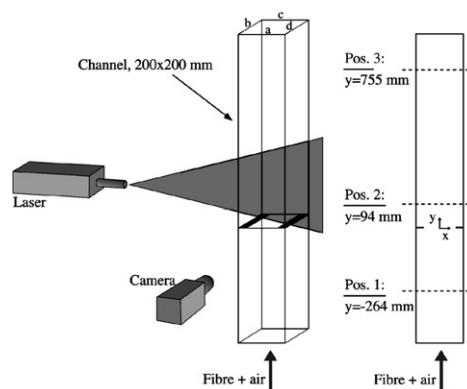

Fig. 1. Experimental set-up. Channel walls marked a and b are transparent. Positions where measurements were taken are marked Pos. 1, Pos. 2 and Pos. 3. The throttle is positioned at $y = 0$ mm, where $x = 0$ mm is at the centre of the throttle.

Table 1
Properties of the wood fibres used in the experiments

Wood species	Pine
Length	1.8 mm
Diameter	29 μm
Coarseness	0.43 mg/m
Curl index	4.9%

Table 2
Parameter settings for the experiments

C (g/m^3)	375 rpm	750 rpm	1500 rpm
25		A	
50		B	
150	C	D	E

The PIV system comprised a Quantel Twins Nd: YAG laser (532 nm), Dantec PIV 2100 processor, Dantec HiSense PIV/PLIF camera and Dantec Flowmanager software. The laser sheet and the camera were set up as indicated in Fig. 1.

The fibres were introduced into the air flow through an opening in the channel located on the suction side of the fan; pine fibres were used for all of the trials. The average moisture content of the fibres was about 10% ($m_w/m_f = 0.1$, m_w = mass of water, m_f = mass of fibre dry substance); other fibre properties are shown in Table 1.

A static eliminator (Walnostat, WA-02) was installed to reduce problems with static electricity building up during the experiments. Water was also sprayed onto the surface of the fibres before their insertion into the air flow. Measurements of the fibre moisture content after a short period of circulation in the channel system indicate that the water evaporates rapidly from the surface of the fibres. The effect of the added water on the fibre density was therefore concluded to be small.

Experiments were performed for three concentration levels and three levels of fan rpm (Table 2). The resulting velocity range of the experiments was about 8–25 m/s (channel average).

2.2. Velocity and concentration measurements

The velocity of the fibres was measured using PIV (Melander and Rasmuson, 2004).

Concentration (volume fraction) measurements were performed using an image processing technique where the average area fraction of fibres in the raw images from the PIV system was determined and converted into volume fraction by the method proposed by Melander and Rasmuson (2004).

Measurements of velocity and concentration were made at three different positions (264 mm before the throttle, 94 and 755 mm after the throttle).

3. Mathematical model

3.1. Model equations

A two-fluid model (e.g. Enwald et al., 1996) was used to simulate the flow of air and fibres. The momentum equations for the gas and fibre phases are given below (Eqs. (1) and (2)). Steady state conditions were assumed for the simulations.

Momentum equation for the gas phase:

$$\frac{\partial}{\partial x_j}\left(\alpha_g\left((\rho_g U_{gi} U_{gj}) - (\mu_g + \mu_{Tg})\left(\frac{\partial U_{gi}}{\partial x_j} + \frac{\partial U_{gj}}{\partial x_i}\right)\right)\right)$$
$$= \alpha_g\left(B_{gi} - \frac{\partial}{\partial x_j}\delta_{ij}p'\right) + K_D(U_{fi} - U_{gi}) - F_i^{TD} - F_i^{LD} \tag{1}$$

Momentum equation for the fibre phase:

$$\frac{\partial}{\partial x_j}\left(\alpha_f\left((\rho_f U_{fi} U_{fj}) - (\mu_f + \mu_{Tf})\left(\frac{\partial U_{fi}}{\partial x_j} + \frac{\partial U_{fj}}{\partial x_i}\right)\right)\right)$$
$$= \alpha_f\left(B_{fi} - \frac{\partial}{\partial x_j}\delta_{ij}p'\right) + K_D(U_{gi} - U_{fi}) + F_i^{TD} + F_i^{SP} + F_i^{LD} \quad (2)$$

α, ρ, U, μ and μ_T are volume fraction, density, velocity, viscosity and turbulent viscosity. B represents body forces such as gravity, K_D is a generalised drag function, F^{TD} is the turbulent dispersion force, F^{LD} is a dispersion force due to lift forces on the fibres and F^{SP} is a solids pressure force. A modified pressure, p', is used in order to obtain the correct trace of the Reynolds stress tensor (CFX 5.7.1 Manual). Indices "f" and "g" indicate fibre or gas phase. Indices i and j indicate vector component. δ_{ij} is the kronecker delta.

A solids pressure model (Gidaspow, 1994) was used to set a restriction on the maximum fibre volume fraction, which was estimated to be 0.07 (loosely packed fibres).

3.2. Drag and lift models

A drag function for fibres orientated at different angles to the air flow (Ju and Shambaugh, 1994) was used to model the interaction between the fibres and the air (Fig. 2). Generalised drag and lift coefficients (Eqs. (3) and (4)) were derived from the expressions for the force on a single fibre (Melander and Rasmuson, 2005). These were subsequently used in the averaged momentum equations of the eulerian–eulerian two-fluid model. An average fibre orientation of 45° was assumed (Melander and Rasmuson, 2005).

$$K_D = \frac{2\rho_g(1-\alpha_g)U_{rel}}{d}\left[C_f \cos^3(\theta) + \frac{C_{DN}}{\pi}\sin^3(\theta)\right] \quad (3)$$

$$K_L = \frac{2\rho_g(1-\alpha_g)U_{rel}}{d}\left[-C_f \cos^2(\theta)\sin(\theta) + \frac{C_{DN}}{\pi}\sin^2(\theta)\cos(\theta)\right] \quad (4)$$

K_D, K_L, U_{rel}, C_f, C_{DN}, d and θ are generalised drag coefficient, generalised lift coefficient, relative velocity, friction coefficient parallel to the fibre axis, drag coefficient normal to the fibre axis, fibre diameter and fibre orientation with respect to the relative velocity vector.

It was concluded in Melander and Rasmuson (2005) that the effect of lift forces (profile lift) cannot be neglected in fibre–gas systems. The quotient of the generalised drag- and lift coefficients (Fig. 3) is a measure of the relative importance of drag and lift forces. It is evident that the lift- and drag forces are of the same order of magnitude for a wide range of flow conditions.

In the present work, a dispersion force was used to model the effect of lift forces acting on individual fibre particles. The dispersing effect of the lift forces, for randomly orientated fibres, is due to statistical processes.
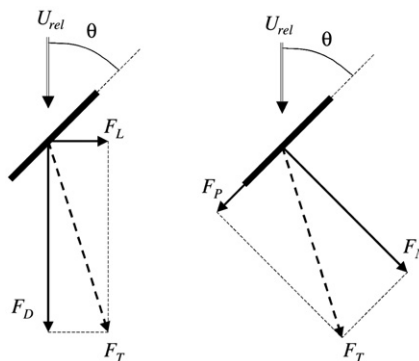

Fig. 2. Forces as defined in the Ju and Shambaugh (1994) drag model. F_D, F_L, F_P, F_N and F_T are drag force, lift force, parallel force, normal force and total force.
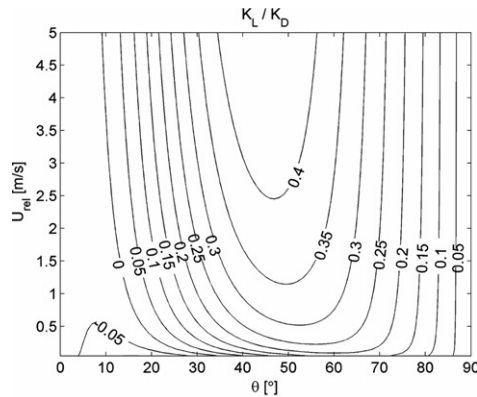
Fig. 3. Quotient of generalised lift and drag coefficient (K_L/K_D) as a function of fibre orientation and relative velocity.
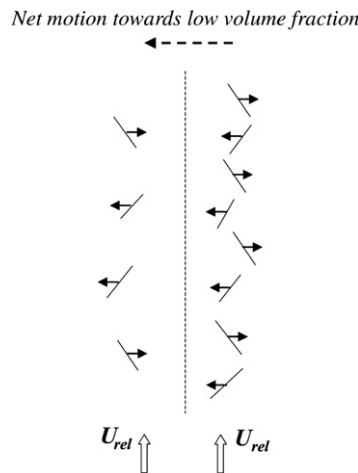

Fig. 4. Mechanism for dispersion due to lift forces acting on individual fibres. More fibres will move from right to left than the other way around.

As shown in Fig. 4, the lift forces acting on the fibres will cause more fibres to move from high to low concentration than the other way around (Melander and Rasmuson, 2005). The size of the lift forces acting on the particles, thus the relative velocity, will also influence the rate of dispersion. The gradient of volume fraction and the relative velocity between the gas and the fibres were therefore identified as important parameters when modelling this phenomenon.

A model for the dispersion force, which incorporates the effect of relative velocity and the volume fraction gradient, is suggested in Eq. (5). Since it is the dispersion of fibres normal to the drag force that is being modelled, the projection of the volume fraction gradient onto the unit lift vector, $\hat{e}_L$, is used in the model.

$$F_i^{LD} = \frac{-C_{LD}K_L}{\alpha_f} U_{rel} \left(\hat{e}_{Lj} \cdot \frac{\partial \alpha_f}{\partial x_j} \right) \cdot \hat{e}_{Li} \qquad (5)$$

A "lift dispersion coefficient", C_{LD}, is required to evaluate the size of the dispersion force; it has the dimension of a length scale.

3.3. Method for obtaining an estimate of C_{LD}

A multi-fluid model with transport equations for fibre orientation, ϕ (with respect to a fixed coordinate system), and angular velocity, ω, was utilised in order to estimate C_{LD}. The motion of a gas phase and ten

fibre-phases, with ten different initial orientations, was simulated. It was possible to set source terms in the momentum equations corresponding to the lift force on each phase since the orientation of each phase was calculated. The dispersing effect of the lift forces was evaluated by studying the development of a "square wave" volume fraction profile (sum of all phases) along a straight channel with flow conditions that were representative for the type of flow in the experimental set-up (Fig. 1). A straight channel was used since it has a very simple geometry where no secondary effects (e.g. recirculation zones, curvature, etc.) affect the dispersion of fibres. Turbulent dispersion was not accounted for in the C_{LD} estimation.

The momentum transfer due to drag and lift forces was two-way coupled, but the transport of orientation and angular velocity was one-way coupled, i.e. the change in angular momentum of the fibres did not result in any sources or sinks in the momentum equations. Only convective transport was included in the transport equations (Appendix 1). This approach would give a good estimate of the dispersing effect of the lift forces for an infinite number of fibre phases. The number of phases was, however, restricted to 10 for reasons of computational power. Simulations were also performed with fewer phases and, since the differences between these simulations and the simulation with 10 phases were small, it was assumed that 10 phases would be sufficient to obtain an estimate of C_{LD}.

The simulations of the gas–fibre flow with transport equations for orientation and angular velocity were compared with two-phase simulations where the lift dispersion force was included. Different values of C_{LD} were tested and a value was determined that gave similar results for both models with regards to fibre dispersion.

3.4. Turbulence and turbulent dispersion

The k–ε model (Launder and Sharma, 1974) was chosen to model the turbulence in the gas phase. The fibre phase turbulence was modelled using a zero equation turbulence model (Lopez de Bertodano, 1998).

Turbulent dispersion of the fibres was modelled using a dispersion force (Lopez de Bertodano, 1998). The dispersion force, F_i^{TD} is given by Eqs. (6) and (7), where k is the turbulence kinetic energy and C_μ is a constant in the k–ε model. The Stokes number, St, is the ratio of fibre relaxation time, τ_f, to the effective turbulent time-scale, τ_g, as defined in Eqs. (8)–(10), where ε is the turbulent dissipation.

$$F_i^{TD} = -C_{TD}\rho_g k_g \frac{\partial \alpha_f}{\partial x_i} \tag{6}$$

$$C_{TD} = \frac{\rho_f}{\rho_g} \frac{1}{St}\left(\frac{1}{1+St}\right)C_\mu^{1/4} \tag{7}$$

$$\tau_f = \frac{\alpha_f \rho_f}{K_D} \tag{8}$$

$$\tau_g = \frac{1}{\sqrt{\frac{1}{\left(c_\mu^{3/4}\frac{k_g}{\varepsilon_g}\right)^2} + \frac{1}{\left(\frac{C_\mu^{1/4}}{2}\frac{k_g^{3/2}}{\varepsilon_g}\frac{1}{U_{rel}}\right)^2}}} \tag{9}$$

$$St = \frac{\tau_f}{\tau_g} \tag{10}$$

4. Numerical

The model equations were solved using the commercial CFD package CFX-5.7.1. Since similar results were obtained for all cases in Table 2 (Melander and Rasmuson, 2005), the simulations and comparison of experimental and numerical data were limited to Case B (Table 2), where the concentration of fibres, C, was 50 g/m^3 and the mass flow of fibres was 25 g/s.

4.1. Geometry and boundary conditions for C_{LD} estimation

The geometry used when estimating the C_{LD} value was a straight two-dimensional channel of width 0.2 m and length 3.3 m (Fig. 6).

The inlet boundary condition was a step in volume fraction centered at the middle of the channel (Fig. 5). The volume fraction of each phase was one tenth of the total fibre volume fraction. A constant velocity boundary condition (13 m/s) was set for the gas phase. The inlet velocity for the fibre phase was set to 10 m/s, i.e. a relative velocity of 3 m/s. In the throttle simulations, the relative velocity is of this order of magnitude close to the throttle, where lift forces can be expected to influence the flow. The wall boundary condition was a slip boundary condition for both phases. The reason for using a slip boundary condition for both phases was to avoid the high shear region and thus the large rotation speed of the fibres associated with a no-slip bondary condition, which could lead to numerical problems. Since the effect of the wall was not important in the estimation of the C_{LD} value this would not affect the simulation results. An outlet boundary condition implying fully-developed flow was used, i.e. gradients normal to the outlet boundary were assumed to be zero. The pressure was set to zero at the outlet. At the inlet, the angular velocity of the fibres was set to zero. The orientations of the different fibre phases are given in Table 3. A fibre orientation, ϕ, of 0° corresponds to the fibre being orientated along the positive x-axis of the geometry. Positive rotation is counter clockwise in the x–y plane.

Symmetry along the middle of the channel ($x = 0$) was utilised in the model with a dispersion force (Fig. 6). It was expected that the average solution, i.e. the average of all fibre phases, would be symmetric for the model with transport equations for orientation and angular velocity. However, since the solution for the individual phases would not be symmetric, the whole width of the channel was modelled (Fig. 6).

4.2. Geometry and boundary conditions for square channel with throttle

It was assumed that three-dimensional effects resulting from the square shape of the channel and previous flow disturbances would be small compared to the effect of the flow deformation in the throttle. A two-dimensional model with a rectangular grid was therefore chosen for the simulations (Fig. 7).
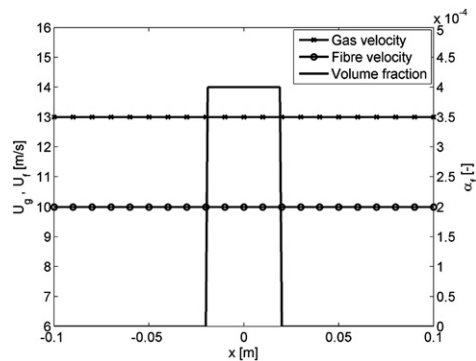

Fig. 5. Inlet volume fraction (fibres) and velocity boundary conditions for C_{LD} estimation.

Table 3
Inlet orientation and volume fraction of the fibre phases

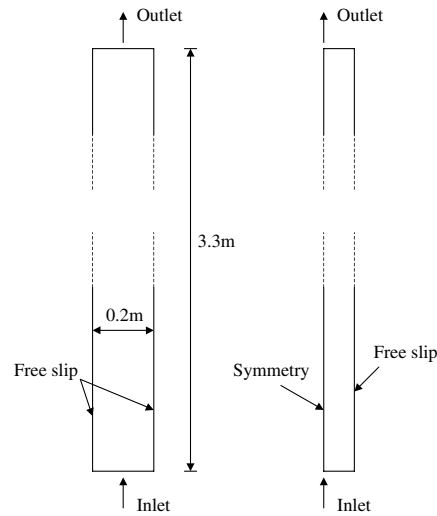| Fibre phase no.	ϕ (°)	α_f (–)
1	15	0.0004/10
2	30	0.0004/10
3	45	0.0004/10
4	60	0.0004/10
5	75	0.0004/10
6	105	0.0004/10
7	120	0.0004/10
8	135	0.0004/10
9	150	0.0004/10
10	165	0.0004/10

Fig. 6. Geometry used for C_{LD} estimation. Left: full geometry. Right: symmetric geometry.
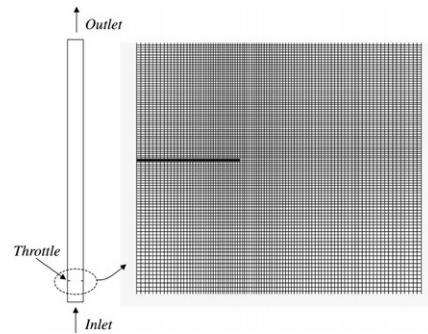

Fig. 7. Model geometry and calculation grid near throttle (left side of channel is shown; thick black line indicates throttle).

In the region near the throttle, the streamwise length-scale of the grid was 0.75 mm and the crosswise length-scale was 0.75–1.5 mm. The mesh was expanded away from the throttle, towards the inlet and outlet. The streamwise length-scale of the mesh was 5 mm at the inlet and 10 mm at the outlet. The total number of cells in the model was about 180,000.

Measured values of volume fraction and velocity of the fibre phase were used as boundary conditions in Position 1. For the gas phase, the inlet normal velocity was set equal to the measured fibre normal velocity adjusted by the terminal velocity (Table 4) of the fibre phase. The cross-stream velocity of both phases was

Table 4
Models and material properties used in the simulations

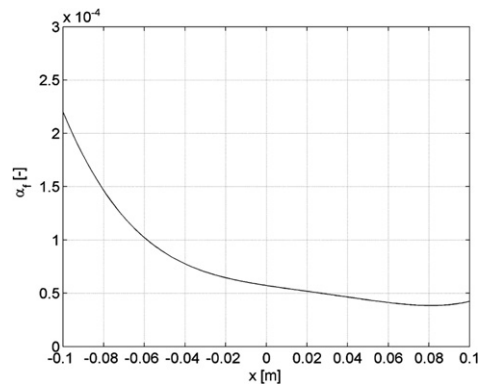| Property/model	Air	Fibres
Viscosity (Pa s)	1.85×10^{-5}	1.0×10^{-8}
Density (kg/m^3)	1.16	715
Length (mm)	–	1.81
Diameter (μm)	–	29.1
Orientation (°)	–	45
Terminal velocity (m/s)	–	0.23
Max. volume fraction (–)	–	0.07
Turbulence model	k–ε	0 Eq. model
Lift dispersion coefficient C_{LD} (m)	–	0.005

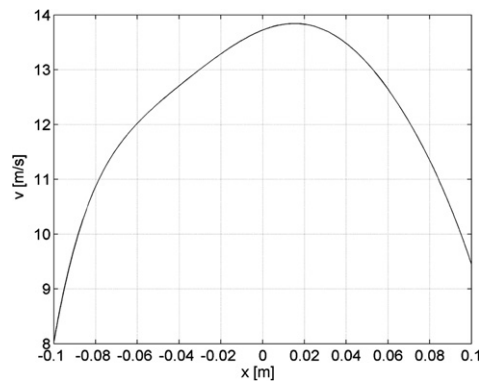Fig. 8. Volume fraction boundary condition for Case B.

Fig. 9. Velocity boundary condition for Case B.

set to zero. The turbulence intensity at the inlet was 3.7%. Symmetric velocity and volume fraction profiles across the channel cross-section could not be obtained in the experiments for practical reasons. Thus, the boundary conditions in the simulations are non-symmetrical. The boundary conditions for Case B are depicted in Figs. 8 and 9.

An outlet boundary condition implying fully-developed flow was used, i.e. gradients normal to the outlet boundary were assumed to be zero. This was not entirely the case in the present calculations but, since the distance from the throttle to the outlet boundary condition was 3.0 m, this was expected to have little effect on the simulation results closer to the throttle. The pressure was set to zero at the outlet.

The wall treatment was a "no slip" boundary condition for the gas phase and a "free slip" boundary condition for the fibre phase.

A summary of the properties of the air, fibres and models that were used in the simulations is given in Table 4.

5. Results and discussion

5.1. Estimation of C_{LD}

A comparison of concentration profiles for the two-fluid model with dispersion force and the model with transport equations for fibre orientation and angular velocity (gas + 10 fibre phases) shows that a reasonable value of the lift dispersion coefficient, C_{LD}, is about 0.005 (Fig. 10).
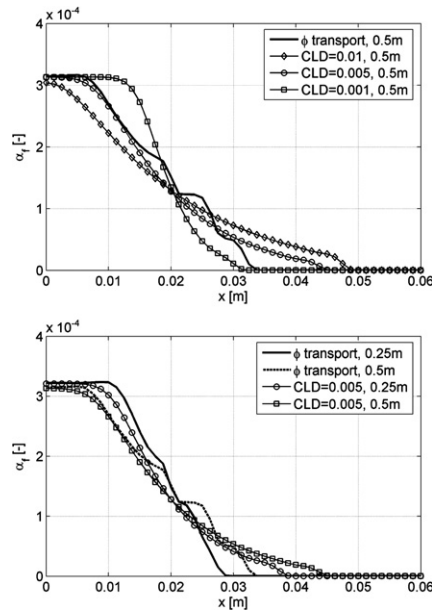
Fig. 10. Comparison of volume fraction profiles along the channel for the model with 10 fibre phases and the model utilising a dispersion force. For resolution purposes, only part of the channel is displayed ($x = 0 \Rightarrow$ center of channel). Upper: volume fraction profile 0.5 m downstream of inlet for different values of C_{LD}. Lower: volume fraction at 0.25 m and 0.5 m downstream of inlet when $C_{LD} = 0.005$.

The concentration profiles are similar in shape for the two models. The fact that the model in which orientation and angular velocity is transported has a finite number of phases is evident from the resulting concentration profile. The "steps" in volume fraction are generated by the discrete levels of initial orientation.

It could be argued that the time averaged lift force on a certain particle should be zero, since the fibre rotation would make the lift force act in opposite directions for the same amount of time. For this to be true, the fibres would have to rotate very quickly and the flow conditions around the fibres not change significantly during one revolution. However, numerical results show that the fibre rotation is sufficiently slow to allow the lift forces to have a dispersing effect. Fig. 11 shows the orientation of a fibre phase with an initial orientation of +45° at different positions along the channel. It can be seen that the lift force vector still has the same direction when the fibre has travelled 0.5 m along the straight channel, since the fibre orientation is still between 0 and 90° (assuming that the relative velocity vector is along the positive *y*-axis). The orientation in part of the cross section is less than 0° after 1.0 m and the lift force thus acts in the opposite direction there. However, the relative velocity between the phases decreases rapidly, resulting in the magnitude of the lift
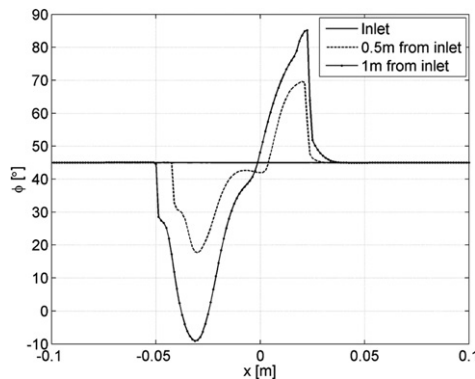

Fig. 11. Orientation, ϕ, of a fibre phase, with an inlet orientation of 45°, at different distances from the inlet.

forces acting on the fibres also decreasing: the relative velocity is reduced by about 90% after just 0.5 m. This means that even if the fibre rotation causes the lift force to act in the opposite direction a certain distance downstream of the position of maximum relative velocity, the magnitude of the forces will be much smaller, thus leaving a net dispersive effect.

5.2. Square channel with throttle

A comparison between CFD results and experimental data is presented below. The difference between the model without lift forces taken into account and a model where the effect of lift forces is modelled as a lift dispersion force is discussed.

5.2.1. Concentration

The sharp peaks in volume fraction that were obtained with the model without lift forces are significantly reduced when the lift dispersion model is used. There are still discrepancies between measurement data and simulation data, although they are much smaller than before. The volume fraction profiles in Positions 2 and 3 are shown in Figs. 12 and 13, respectively.

There is most likely a smoothing effect in the measurement data caused by jet oscillation, which was observed in the measurements. The effect of this should be largest in Position 3, and could explain the large difference between experimental data and numerical results in this position.
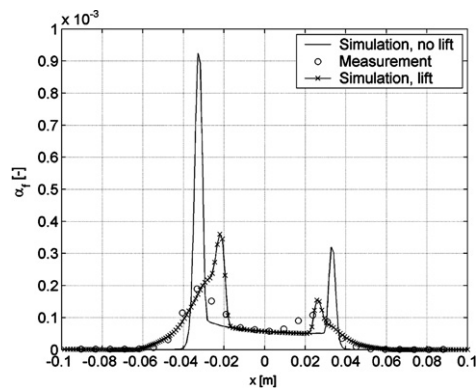

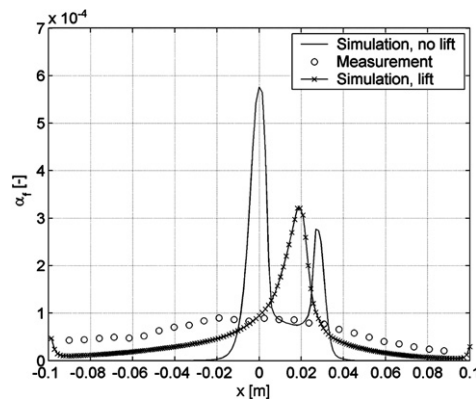Fig. 12. Measured and simulated volume fraction profile in Position 2.

Fig. 13. Measured and simulated volume fraction profile in Position 3.

In the region close to Position 2, where the lift forces are expected to have the most influence on fibre dispersion, the lift dispersion force is about 400 times larger than the turbulent dispersion force modelled according to Lopez de Bertodano (1998). Near Position 3, the lift and turbulent dispersion forces are of the same order of magnitude. The absolute size of the lift dispersion force is about 10 times larger in Position 2 than in Position 3.

5.2.2. Velocity

The use of a dispersion force did not markedly improve the agreement between measurement data and numerical data for velocity (Figs. 14–17). In some cases, the results were worse than without the use of the
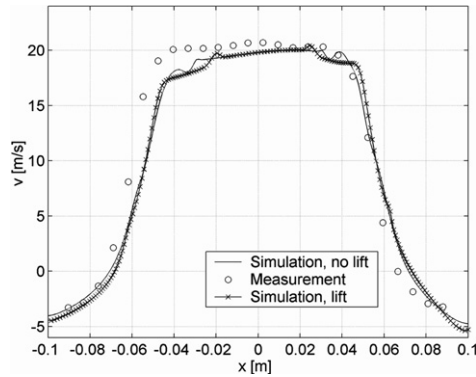
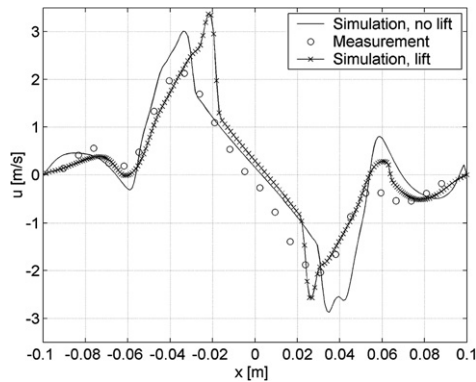Fig. 14. Measured and simulated v-velocity in Position 2.

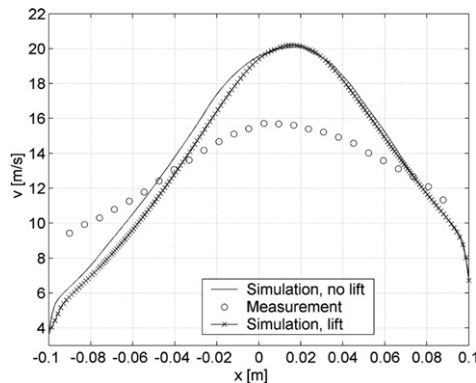Fig. 15. Measured and simulated u-velocity in Position 2.

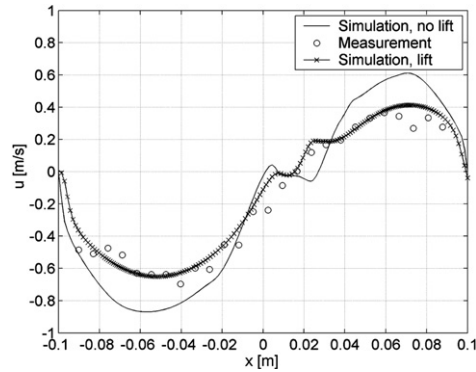Fig. 16. Measured and simulated v-velocity in Position 3.

Fig. 17. Measured and simulated u-velocity in Position 3.

dispersion force model (e.g. Fig. 16). The oscillation of the jet, which was observed in the experiments, could be the reason for the poor agreement between measured and numerical data.

6. Conclusions

The results from this study indicate that the dispersing effect of lift forces acting on the individual fibres is not negligible. It is a real effect and it should be included in the model equations in order to obtain an accurate solution. A reasonable value of the lift dispersion coefficient is 0.005.

The results obtained from the model in which fibre orientation and angular velocity are transported show that the fibres rotate considerably. The rotation is, however, slow enough to make the dispersive effect of lift forces significant.

In the present work, a dispersion force approach was used and a significant improvement over previous results was obtained close to the throttle (Position 2). In the region further downstream of the throttle (Position 3), jet oscillation probably has a significant contribution to the discrepancy between measured and numerical data.

Acknowledgement

Appendix 1

Transport equation for fibre orientation, ϕ

$$\frac{\partial}{\partial x_j}(\alpha_f U_{fj}\phi_f) = S_f^{(\phi)} \tag{A.1}$$

$$S_f^{(\phi)} = \alpha_f \omega \tag{A.2}$$

Transport equation for fibre angular velocity, ω

$$\frac{\partial}{\partial x_j}(\alpha_f U_{fj}\omega_f) = S_f^{(\omega)} \tag{A.3}$$

$$S_f^{(\omega)} = \alpha_f \dot{\omega} \tag{A.4}$$

where the angular acceleration is given by

$$\dot{\omega} = \frac{M}{J} \tag{A.5}$$

and the moment of inertia, J, is calculated as

$$J = \frac{mL^2}{12} \tag{A.6}$$

where m and L are the fibre mass and fibre length.

The moment, M, on the fibre is approximated as

$$M = \frac{L^2}{12}(f_{N,L/2} - f_{N,-L/2}) \tag{A.7}$$

where $f_{N,L/2}$ and $f_{N,-L/2}$ is the force per unit length at each end of the fibre.

The force per unit length at each end is obtained by using the Ju and Shambaugh (1994) drag function. The relative velocities at the two endpoints of every fibre are calculated by assuming that the gas velocity gradient is constant along each fibre and that the fibres rotate as stiff cylinders with length L.

References

CFX, 5.7.1 Manual, ANSYS-CFX.

Cox, R.G., 1970. The motion of long slender bodies in a viscous fluid. I. General theory. J. Fluid Mech. 44, 791–810.

Ek, R., Moller, K., Norman, B., 1978. Measurement of velocity and concentration variations in dilute fiber–air suspensions using a laser doppler anemometer. Tappi 61, 49–52.

Enwald, H., Peirano, E., Almstedt, A.E., 1996. Eulerian two-phase flow theory applied to fluidization. Int. J. Multiphase Flow 22, 21–66.

Garner, R.G., Kerekes, R.J., 1980. Flow regimes of wood pulp fibers in air suspensions. Tappi 63, 103–107.

Gidaspow, D., 1994. Multiphase Flow and Fluidisation. Academic Press, Boston.

Jeffery, G.B., 1922. The motion of ellipsoidal particles immersed in a viscous fluid. Proc. R. Soc. Ser. A 102, 161–179.

Ju, Y.D., Shambaugh, R.L., 1994. Air drag on fine filaments at oblique and normal angles to the air stream. Polym. Eng. Sci. 34, 958–964.

Launder, B.E., Sharma, B.I., 1974. Application of the energy-dissipation model of turbulence to the calculation of flow near a spinning disc. Lett. Heat Mass Transfer 1, 131–137.

Ljus, C., 2000. On particle transport and turbulence modification in air-particle flows, Ph.D. thesis, Department of Thermo and Fluid Dynamics, Chalmers University of Technology.

Ljus, C., Almstedt, A.E., 1999. Eulerian Modelling of Pulp-Fibre Transport in Airflow, Two-Phase Flow Modelling and Experimentation 1999, Pisa, Edizioni ETS.

Ljus, C., Johansson, B., Almstedt, A.-E., 2002. Turbulence modification by particles in a horizontal pipe flow. Int. J. Multiphase Flow 28, 1075–1090.

Lopez de Bertodano, M.A., 1998. Two fluid model for two-phase turbulent jets. Nucl. Eng. Des. 179, 65–74.

Mason, S.G., 1950. The motion of fibres in flowing liquids. Pulp Paper Mag. Can., 93–100.

Melander, O., Rasmuson, A., 2004. PIV measurements of velocities and concentrations of wood fibres in pneumatic transport. Exp. Fluids 37, 293–300.

Melander, O., Rasmuson, A., 2005. Simulation and measurement of velocity and concentration of dry wood fibres flowing through a throttle. Nordic Pulp Paper Res. J. 20, 78–86.

Melander, O., Wikstrom, T., Rasmuson, A., 2006. Flow regimes of air suspensions of MDF fibres in vertical flow. Nordic Pulp Paper Res. J. 21, 227–230.

Olson, J.A., 2001. The motion of fibres in turbulent flow, stochastic simulation of isotropic homogeneous turbulence. Int. J. Multiphase Flow 27, 2083–2103.

Olson, J.A., Kerekes, R.J., 1998. The motion of fibres in turbulent flow. J. Fluid Mech. 377, 47–64.